© 2021 IEEE. Personal use of this material is permitted. Permission from IEEE must be obtained for all other uses, in any current or future media, including reprinting/republishing this material for advertising or promotional purposes, creating new collective works, for resale or redistribution to servers or lists, or reuse of any copyrighted component of this work in other works.

Rapid Power Compensation Based Frequency Response Strategy for Low Inertia Power Systems

Liansong Xiong, *Member, IEEE,* Xiaokang Liu, *Member, IEEE,* Donghui Zhang, and Yonghui Liu, *Student Member, IEEE*

***Abstract*—To reduce the frequency deviation and the rate of change of frequency (RoCoF) in a low inertia power system, some converters are required to provide the frequency response (FR) power normally associated with the frequency deviation and/or the RoCoF, by droop/inertia/PD control. In this article, a rapid power compensation (RPC) based FR strategy is developed to optimize the ability to compensate grid imbalance power, by fully exploiting the converter idle capacity. To this end, first, mathematical proof demonstrated the improved performance of the RPC strategy in terms of frequency deviation suppression versus droop control, and in terms of RoCoF suppression versus inertia control, with identical converter capacity limit. Moreover, it is proved that the RPC strategy can achieve consistent FR performance with respect to the optimal PD control, i.e. it can maximize the suppression of frequency deviation and RoCoF simultaneously, yet avoiding the limitations due to unknown grid parameters. Finally, by analyzing the operation modes and identifying the pertinent switching logic, the detailed implementation of the proposed RPC strategy is developed. Its superb FR performance is verified by the experiment results in a two-converter low-inertia system, and simulation results in an IEEE four-machine two-area system.**

***Index Terms*—Frequency deviation, frequency response (FR), grid-tied converter, low inertia power system, rate of change of frequency (RoCoF), rapid power compensation (RPC).**

I. Introduction

THE utility grid frequency is one of the basic indicators for power quality assessment and the only one that reflects the power supply and demand balance [1]. For the safe and stable operation of the utility grid, a constant frequency equal to grid synchronous frequency (usually 50 or 60 Hz) is required. Nevertheless, long-term utility operation suffers from a variety of power disturbances that would cause the grid frequency to deviate from the nominal value. A significant frequency deviation as well as the rate of change of frequency (RoCoF) can cause a series of adverse consequences [2], and some explanatory examples encompass excessive mechanical torque causing the synchronous generator (SG) shaft to fatigue or even break; motor speed perturbation causing defective products on the production line; performance degradation of the frequency-sensitive instrument resulting in measurement error; a frequency nadir lower than 46/47 Hz significantly affecting the thermal power plant operation, leading to low-frequency tripping, long-term power shortage and eventually frequency collapse; a frequency nadir lower than 45/46 Hz causing the generator speed and excitation to significantly reduce and electromotive force to drop; and finally, notable grid voltage sag (or even worse, voltage collapse). Large-scale power outages, e.g. the September 28 blackout in Australia, 2016 [3], and the August 9 blackout in U.K., 2019, are inevitable in the event of frequency/voltage collapse.

To avoid the aforementioned frequency stability issues, the frequency deviation and RoCoF are regulated by the grid code in many countries. Once an indicator exceeds its pertinent threshold for a certain time duration, the under-/over-frequency relay or RoCoF relay will be triggered. As illustrative examples, the frequency nadir limits specified in Ireland, Australia, United States, and Great Britain, are 47.5, 47.5, 59.3 (with 60 Hz-nominal frequency), and 49.5 Hz, respectively [2]. Typical RoCoF relay settings (see Tab. I for standards in several countries) range from 0.1 to 1.0 Hz/s in 50-Hz power systems and from 0.12 to 1.2 Hz/s in 60-Hz power systems [4].

The SGs are characterized by large inertia, strong damping ability, and frequency response (FR) characteristics, namely, the output power can be adjusted autonomously on grid frequency change [7]. Accordingly, conventional SGs-based power systems have relatively robust grid frequency, with frequency deviation and RoCoF readily satisfying grid code requirements. Nevertheless, for a converter-dominated system, most of the interface devices between the grid and primary energy/terminal load are based on various power converters [8], which are commonly considered to have low (or null) inertia and weak damping ability; in the presence of a disturbance, frequency deviation and RoCoF relays can easily trigger [3]. Due to the growing converter-based generations and loads, RoCoF relay thresholds in many countries have been compromised (see Table I).

Meanwhile, increasing efforts are being made to seek larger

Manuscript received May 19, 2020; revised August 20, 2020 and October 4, 2020; accepted October 12, 2020. *(Corresponding author: Xiaokang Liu.)*

This work was supported in part by the National Natural Science Foundation of China under Grant 51707091, in part by the State Key Laboratory of Alternate Electrical Power System with Renewable Energy Sources under Grant LAPS19008, and in part by the Key Laboratory of Control of Power Transmission and Conversion (SJTU), Ministry of Education under Grant 2018AC04.

L. Xiong is with the School of Automation, Nanjing Institute of Technology, Nanjing 211167, China and also with the School of Electrical Engineering, Xi'an Jiaotong University, Xi'an 710049, China (e-mail: xionglian-song@163.com).

X. Liu is with the Department of Electronics, Information and Bioengineering, Politecnico di Milano, 20133 Milano, Italy and also with the School of Electrical Engineering, Xi'an Jiaotong University, Xi'an 710049, China (e-mail: xiaokang.liu@polimi.it).

D. Zhang is with the College of Automation Engineering, Nanjing University of Aeronautics and Astronautics, Nanjing 211106, China (e-mail: ceozdhceo@163.com).

Y. Liu is with the School of Electrical Engineering, Xi'an Jiaotong University, Xi'an 710049, China (e-mail: liuyonghui@stu.xjtu.edu.cn).

TABLE I
ROCOF RELAY STANDARDS IN SOME COUNTRIES (WITH NOMINAL FREQUENCY OF 50 HZ) [5], [6].

Country	RoCoF relay (before)	RoCoF relay (updated)
Ireland	0.5 Hz/s	1.0 Hz/s
Great Britain	0.125 Hz/s	0.5 Hz/s
Denmark	0.8 Hz/s	2.5 Hz/s
Spain	0.4 Hz/s	2.0 Hz/s
South Africa	0.5 Hz/s	1.5 Hz/s
Finland	0.75 Hz/s	2.0 Hz/s
Belgium	/	1.0 Hz/s
Cyprus	/	0.6 Hz/s
Latvia	/	0.4 Hz/s

FR power and reduce the RoCoF and frequency deviation in low-inertia systems, encompassing 1) adopting physical SG-based generations and 2) employing virtual SG (VSG) schemes for grid-tied converters. Typical physical SG-based schemes include 1) the concentrating solar power scheme that utilizes solar thermal power to generate electricity [9], [10] and 2) the synchronous motor–generator pair scheme, in which the renewable energy drives a synchronous motor, and, subsequently, a grid-tied SG [7], [11]. In both cases, physical SGs are utilized for providing inertia and FR power to the grid. With the SGs being replaced by power converters in modern power systems, the FR schemes resorting to VSG techniques for converter-based generations and loads become the mainstream of research and application. The virtual synchronous machine [12], synchronverters [13], synchronous power control [14] and generalized droop control [15] are the typical VSG schemes that emulate the inertia response and maintain frequency stability of the low-inertia system by exploiting the swing-equation-based SG model. However, when inverters with swing-equation-based VSG control are connected to the utility grid integrated with physical SGs, power and frequency oscillations will occur due to the mismatch of rotational inertia and other parameters of the utility grid [16], severely jeopardizing the grid frequency stability. When the oscillation amplitude exceeds a certain range, the inverters must stop working for protection.

To alleviate the oscillations and obtain better FR performance, various adaptive VSG strategies have been proposed. The self-tuning VSG in [17] and [18] can greatly reduce the FR power or achieve the optimal FR performance. However, obtaining the optimal inertia and damping coefficients requires the online solution of an optimization problem [19], which cannot be well implemented in embedded controller-based inverter systems. The VSG with alternating inertia proposed in [20] exhibits remarkable performance in fast damping of oscillations, yet it neglects the effect of damping factor [19]. Though the self-adaptive inertia and damping controls in [16] and [19] fully consider the relationship between frequency stability and its parameters, how to design the critical parameters that determine the VSG performance is unclear. The optimal inertia and damping parameters that reduce the oscillation amplitude and maintain the stability can be obtained via optimization [21], yet its solution requires detailed SGs' parameters and line impedances that are mostly unknown. It is outlined in [22] that VSG and droop controls are equivalent under certain conditions. On basis of that, Meng *et al.* [15] propose the generalized droop control that functions as a combination of droop control and VSG control, yet requiring complicated controller design and easily causing complex oscillations in the grid-tied mode. As an alternative, the proportional-derivative (PD) controller embedded FR schemes avoid the use of the SG model and effectively mitigate such complex oscillations, and hence, they dominate the industrial applications [23]–[25].

In essence, the aforementioned schemes can lower the frequency deviation and RoCoF since converter based generations contribute to additional FR power, normally proportional to the frequency deviation, and/or RoCoF, which counteracts the grid imbalance power. Indeed, the classic droop control, inertia control and PD control are intensively applied in industry to achieve such an FR power supply and can act as the simplified models for other FR schemes [22]–[25]. Albeit increasing controller gains theoretically indicates more FR power and a further reduction in the frequency deviation and RoCoF, there are following technical challenges to be effectively solved.

1) The major capacity of a grid-tied converter is utilized for transmitting required electric power to the utility/load, leaving an extremely limited available capacity for FR service. Increasing controller gains without protection can easily cause over-current faults. With this consideration in place, how to maximize the reduction in frequency deviation and RoCoF has emerged as a particularly concerning issue.
2) With the limited FR service capacity, the issues of complex power oscillation and poor FR performance are unavoidable for swing-equation-based VSG controls. In this case, the system behavior can be worse than that without the FR service, and the power system can even lose synchronization [26]–[28].
3) The optimal parameters of FR schemes are influenced by unknown parameters such as the grid inertia/damping coefficients and the disturbance to grid. Moreover, different control parameters are often required under various working conditions. Therefore, the optimal FR cannot be directly achieved once and for all.

In this paper, a rapid power compensation (RPC)-based scheme for converter-based generations/loads is developed for improved FR performance, accounting for the limit of converter FR capacity. The major contributions encompass the following.

1) Optimal FR performance is achieved by the proposed FR strategy, decoupling the converter FR power from frequency deviation/RoCoF, and fully exploiting the available converter capacity to compensate for the grid imbalance power;
2) The enhanced performance of the proposed strategy in terms of frequency deviation/RoCoF suppression with respect to the classic controls is justified by rigorous mathematical proof under the same physical constraint;

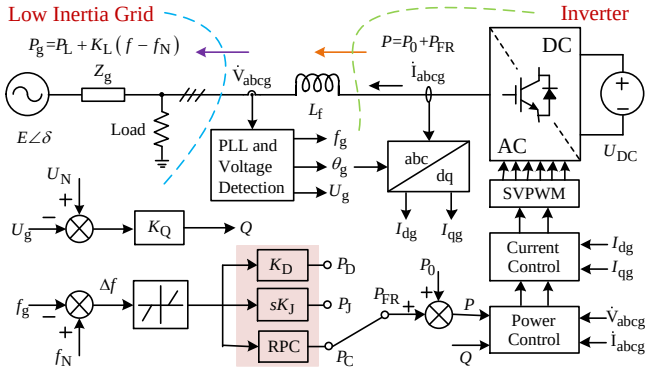

Fig. 1. Studied power system and typical FR strategies. L_f is the passive filter inductance of inverter, and Z_g denotes the grid equivalent impedance that is usually resistive-inductive, i.e. $Z_g = R_g + jX_g$ [29].

3) By analyzing the operation modes and their switching mechanism, detailed implementation of the proposed strategy, which is free from those unknown grid parameters and the complex power oscillations, is obtained;
4) The adaptability and superiority of the proposed scheme are verified by experiment and simulation results under different conditions of grid system topology and disturbance type.

The remainder of this paper is as follows. In Section II, the FR processes of a low-inertia power system with typical FR schemes and the proposed RPC strategy are modeled and comparatively analyzed. In Section III, the detailed implementation of the proposed RPC based FR strategy is developed, and its pertinent operation modes are analyzed. FRs of different control schemes are compared in Section IV, verifying the effectiveness of the proposed technique in various scenarios. Conclusions are finally drawn in Section V.

II. RPC Based FR Strategy: Principle and Mathematical Proof of Improved Performance

A. Necessity of FR Service

Without loss of generality, a power grid with one converter (see Fig. 1) is studied. The system frequency dynamic process is determined by the imbalance power P_{im} between the converter output P and grid absorption P_g [26], yielding

$$T_J \frac{df}{dt} = P_{im} = P - P_g \tag{1}$$

with $T_J = 4\pi H$ and H the system inertia constant.

In steady state, it holds that $P = P_g$. If power imbalance occurs (namely, $P \neq P_g$) due to a power disturbance ΔP_L, the grid frequency f then deviates from its rated value f_N (50/60 Hz) and keeps dropping/rising/oscillating until power balance is reached. With low inertia (H) and/or large disturbance (ΔP_L), the frequency deviation and RoCoF that are representative for system dynamics can easily exceed the pertinent limit, and thus triggering the frequency-related protection and control devices (e.g., underfrequency load shedding and generator disconnection) reluctantly.

Under the same disturbance, it's more challenging to maintain frequency stability in a low inertia system. In such a case, instead of operating in the constant power mode, converter-based generations and loads are required to additionally provide enough FR power P_{FR} to the grid, as such mitigating the frequency deviation caused by P_{im}. With the FR service enabled, the actual converter output power P yields

$$P = P_0 + P_{FR} \tag{2}$$

where P_0 is the steady-state output power of converter based generations when $\Delta P_L = 0$ and $f = f_N$.

In addition to the FR service provided by converter-based generations, a power system is characterized by its intrinsic FR features (e.g. asynchronous motor loads automatically increase their consumption power as frequency rises) described by

$$P_g = P_L - K_L (f_N - f) \tag{3}$$

where P_L is the grid absorption power in steady state and K_L is the grid intrinsic FR coefficient.

In the event of a power disturbance, the FR power provided by the converter and grid reacts to the frequency change by compensating for the imbalance power. If the imbalance power is annihilated instantaneously, virtually no frequency deviation or RoCoF issue will be observed. Assuming the grid load power to be suddenly increased by ΔP_L (i.e., $P_L = P_{L0} + \Delta P_L$), frequency dynamics in (1) can be rewritten, by considering the total FR power of the converter and grid, as (where $P_0 = P_{L0}$):

$$T_J \frac{df}{dt} = (P_0 + P_{FR}) - [P_{L0} + \Delta P_L - K_L (f_N - f)]. \tag{4}$$

It is obvious that when $\Delta P_L = 0$ and $f = f_N$, it is $P_{FR} = 0$. For $\Delta P_L \neq 0$, the frequency deviation and RoCoF levels are greatly influenced by the FR power from the converter, P_{FR}. If few converters respond to grid frequency events and provide the FR service, the power system would lack enough FR power to counteract the imbalance power, causing large frequency deviation/RoCoF values and further consequences. Therefore, in low inertia power systems, converter based generations and loads should actively provide the FR service and maintain the system frequency stability as a collaborative effort. With reference to (4), for $\Delta P_L > P_{FR}$, the RoCoF decreases with larger P_{FR}. Accordingly, to significantly reduce the frequency deviation and RoCoF and avoid frequency-relevant issues, the FR service should increase P_{FR} to its maximum extent.

In passing, it is worth mentioning that the analysis of frequency dynamic process neglects the fast dynamics of high-bandwidth current/power control loops and the phase-locked loop. Indeed, it is a common practice to view these loops as proportional gains in a similar application [30], due to the significantly smaller time constant of the control system with respect to the frequency and the principle of bandwidth zoning for designing the dual-controller loops.

B. Typical FR Schemes and Proposed RPC Strategy

1) Typical FR schemes: As shown in Fig. 2, the FR power provided by the converter of generations is generally proportional to the frequency deviation (droop control) or the RoCoF (inertia control). The corresponding FR power can be

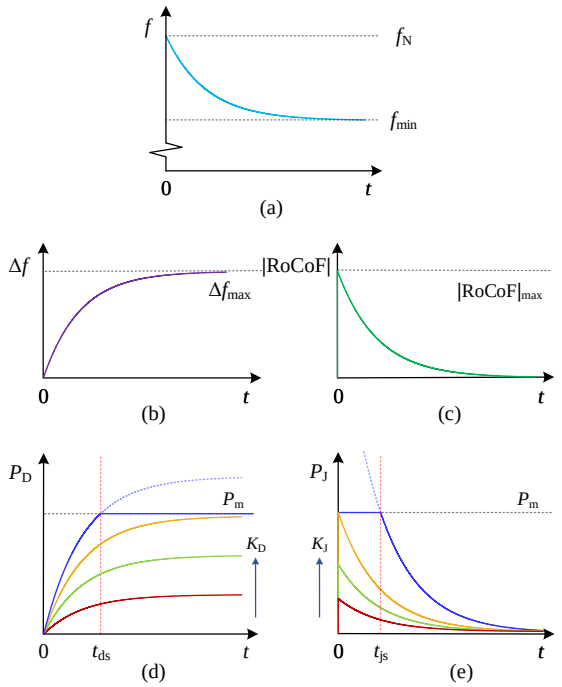

Fig. 2. Behaviors of two typical FR strategies in the event of a frequency drop. (a)-(c): Frequency dynamics, frequency deviation and absolute RoCoF. (d) and (e) Converter FR power with droop and inertia control, respectively.

formulated as (with K_D and K_J the droop and inertia controller gains, respectively; s being the derivative operator):

$$P_D = K_D\left(f_N - f\right) \tag{5}$$

$$P_J = sK_J\left(f_N - f\right). \tag{6}$$

The FR power increases with 1) frequency deviation and RoCoF and 2) controller gains K_D and K_J, as illustrated in Fig. 2(d) and (e). Considering the limited converter capacity for FR service, the abovementioned FR schemes are analyzed as follows.

Droop Control: At the initial stage of frequency dynamics, the insignificant frequency deviation leads to limited converter FR output power [see the interval $(0, t_{ds})$ in Fig. 2(d)], which is insufficient for a large power disturbance. To adequately compensate for ΔP_L and avoid further issues, the controller gain K_D should be increased to compress the interval $(0, t_{ds})$, yet the frequency deviation near the nadir can cause P_{FR} to exceed the converter capacity limit [see the dotted blue line in (t_{ds}, t_∞), Fig. 2(d)]. This can be effectively solved by exploiting the saturation state with constant output power P_m equal to the maximum allowable FR power of the generation, as such guaranteeing the converter stable operation and avoiding over-current faults.

Inertia Control: Conversely, P_{FR} at the beginning is relatively large according to the RoCoF [see Fig. 2(c) and (e)]. In $(0, t_{js})$, the same saturation mechanism is adopted for P_{FR}, and the saturation range extends (i.e. the maximum FR power retains for a longer time, providing stronger RoCoF suppression ability) with larger K_J. However, P_{FR} becomes negligible for frequency dropping near its nadir, where the FR service is insufficient for controlling the enlarged frequency deviation, and the underfrequency relay can be easily triggered.

PD Control: Comparing the FR strategy working profiles, it is seen that the droop control performs better for frequency deviation suppression, while the inertia control is advantageous for RoCoF suppression. To achieve good performance in both cases, a combination of the two FR schemes has been made, forming the basic PD control embedded FR scheme introduced in Section I. Accordingly, the FR power is given by (with K_p and K_d being the proportional and derivative gains, respectively)

$$P_{PD} = \left(K_p + sK_d\right)\left(f_N - f\right). \tag{7}$$

2) Proposed RPC based FR scheme: In this article, an RPC-based FR strategy is developed to seek more FR power, yet avoiding possible overcurrent faults and complex oscillations. As a basic principle, the proposed method widens the saturation interval to the entire FR service period, namely, the converter available capacity P_m is fully exploited to provide the FR power and quickly compensate for the system disturbance power ΔP_L ($P_m < \Delta P_L$). A reduced imbalance power after compensation contributes to more robust system frequency, i.e., smaller frequency deviation and RoCoF values.

The previously mentioned FR strategies foresee the generation of FR power proportional to the frequency deviation or RoCoF. This does no longer occur for the proposed RPC-based FR strategy aimed at maximizing the compensation of grid imbalance power, with which the maximum allowable level of FR power (positive or negative) is directly adopted.

C. FR Strategies Comparison

In the analyses hereinafter, the available converter capacity for FR service is considered identical (i.e. $P_{FR} \le P_m < \Delta P_L$). Besides, linear operation (without saturation) is presumed for the pure droop/inertia/PD control.

First, by considering $P_0 = P_{L0}$, (4) can be simplified as

$$T_J\frac{df}{dt} = P_{FR} + K_L\left(f_N - f\right) - \Delta P_L. \tag{8}$$

Adopting the RPC based FR strategy for the converter, the grid frequency dynamic process writes (with $P_{FR} = P_m$)

$$T_J\frac{df_C}{dt} = P_m + K_L\left(f_N - f_C\right) - \Delta P_L. \tag{9}$$

The solution of the grid frequency yields

$$f_C = f_N - \frac{\Delta P_L - P_m}{K_L}\left(1 - e^{-\frac{K_L}{T_J}t}\right). \tag{10}$$

The frequency deviation and RoCoF in such a case can be further derived as

$$\Delta f_C = f_N - f_C = \frac{\Delta P_L - P_m}{K_L}\left(1 - e^{-\frac{K_L}{T_J}t}\right) \tag{11}$$

$$R_C = \frac{df_C}{dt} = -\frac{\Delta P_L - P_m}{T_J}e^{-\frac{K_L}{T_J}t}. \tag{12}$$

1) RPC Versus Droop Control: Adopting the droop control based FR strategies for the converter, the frequency dynamic equation can be obtained by combining (5) and (8), as

$$T_J\frac{df_D}{dt} = \left(K_D + K_L\right)\left(f_N - f_D\right) - \Delta P_L. \tag{13}$$

The grid frequency, frequency deviation and RoCoF can be solved, respectively, as

$$f_{\mathrm{D}} = f_{\mathrm{N}} - \frac{\Delta P_{\mathrm{L}}}{K_{\mathrm{L}} + K_{\mathrm{D}}} \left(1 - e^{-\frac{K_{\mathrm{L}}+K_{\mathrm{D}}}{T_{\mathrm{J}}} t}\right) \tag{14}$$

$$\Delta f_{\mathrm{D}} = \frac{\Delta P_{\mathrm{L}}}{K_{\mathrm{L}} + K_{\mathrm{D}}} \left(1 - e^{-\frac{K_{\mathrm{L}}+K_{\mathrm{D}}}{T_{\mathrm{J}}} t}\right) \tag{15}$$

$$R_{\mathrm{D}} = -\frac{\Delta P_{\mathrm{L}}}{T_{\mathrm{J}}} e^{-\frac{K_{\mathrm{L}}+K_{\mathrm{D}}}{T_{\mathrm{J}}} t} \tag{16}$$

Considering the power limit [see (5) and (15)], the controller gain K_{D} is constrained as

$$P_{\mathrm{D}}|_{\max} = K_{\mathrm{D}} \Delta f_{\mathrm{D}}|_{\max} = \frac{\Delta P_{\mathrm{L}} K_{\mathrm{D}}}{K_{\mathrm{L}} + K_{\mathrm{D}}} \leq P_{\mathrm{m}}. \tag{17}$$

To achieve the optimal droop control that provides the maximum FR power, it is

$$K_{\mathrm{D}} = \frac{K_{\mathrm{L}} P_{\mathrm{m}}}{\Delta P_{\mathrm{L}} - P_{\mathrm{m}}}. \tag{18}$$

By substituting (18) into (15) and comparing with (11), it holds that (considering $t > 0$ hereinafter)

$$\Delta f_{\mathrm{D}} - \Delta f_{\mathrm{C}} = \frac{\Delta P_{\mathrm{L}} - P_{\mathrm{m}}}{K_{\mathrm{L}}} e^{-\frac{K_{\mathrm{L}}}{T_{\mathrm{J}}} t} \left(1 - e^{-\frac{K_{\mathrm{D}}}{T_{\mathrm{J}}} t}\right) > 0. \tag{19}$$

Comparison of the maxima in (12) and (16) yields

$$|R_{\mathrm{D}}|_{\max} - |R_{\mathrm{C}}|_{\max} = \frac{P_{\mathrm{m}}}{T_{\mathrm{J}}} > 0. \tag{20}$$

Equations (19) and (20) highlight the improved performance of the RPC based FR strategy with respect to the droop control, for suppressing the frequency deviation and maximum RoCoF. The suppression ability for maximum RoCoF can be further improved with a larger converter idle capacity P_{m}.

2) RPC Versus Inertia Control: By substituting (6) into (8), the grid frequency, frequency deviation and RoCoF under the inertia control-based FR strategy can be obtained as

$$f_{\mathrm{J}} = f_{\mathrm{N}} - \frac{\Delta P_{\mathrm{L}}}{K_{\mathrm{L}}} \left(1 - e^{-\frac{K_{\mathrm{L}}}{T_{\mathrm{J}}+K_{\mathrm{J}}} t}\right) \tag{21}$$

$$\Delta f_{\mathrm{J}} = \frac{\Delta P_{\mathrm{L}}}{K_{\mathrm{L}}} \left(1 - e^{-\frac{K_{\mathrm{L}}}{T_{\mathrm{J}}+K_{\mathrm{J}}} t}\right) \tag{22}$$

$$R_{\mathrm{J}} = -\frac{\Delta P_{\mathrm{L}}}{T_{\mathrm{J}} + K_{\mathrm{J}}} e^{-\frac{K_{\mathrm{L}}}{T_{\mathrm{J}}+K_{\mathrm{J}}} t}. \tag{23}$$

According to (6) and (23), K_{J} is constrained as

$$P_{\mathrm{J}}|_{\max} = K_{\mathrm{J}} \left.\frac{d\Delta f_{\mathrm{J}}}{dt}\right|_{\max} = \frac{\Delta P_{\mathrm{L}} K_{\mathrm{J}}}{T_{\mathrm{J}} + K_{\mathrm{J}}} \leq P_{\mathrm{m}}. \tag{24}$$

To achieve the optimal inertia control with the maximum FR power while avoiding saturation, we have

$$K_{\mathrm{J}} = \frac{T_{\mathrm{J}} P_{\mathrm{m}}}{\Delta P_{\mathrm{L}} - P_{\mathrm{m}}}. \tag{25}$$

Substituting (25) into (23) and comparing with (12), it is

$$|R_{\mathrm{J}}| - |R_{\mathrm{C}}| = \frac{\Delta P_{\mathrm{L}} - P_{\mathrm{m}}}{T_{\mathrm{J}}} e^{-\frac{K_{\mathrm{L}}}{T_{\mathrm{J}}} t} \left(e^{\frac{K_{\mathrm{L}}}{T_{\mathrm{J}}} \frac{P_{\mathrm{m}}}{\Delta P_{\mathrm{L}}} t} - 1\right) > 0. \tag{26}$$

Similarly, by combining (11), (22) and (25), it holds that

$$\Delta f_{\mathrm{J}} - \Delta f_{\mathrm{C}} = \frac{P_{\mathrm{m}}}{K_{\mathrm{L}}} - \frac{\Delta P_{\mathrm{L}}}{K_{\mathrm{L}}} e^{-\frac{K_{\mathrm{L}}}{T_{\mathrm{J}}+K_{\mathrm{J}}} t} + \frac{\Delta P_{\mathrm{L}} - P_{\mathrm{m}}}{K_{\mathrm{L}}} e^{-\frac{K_{\mathrm{L}}}{T_{\mathrm{J}}} t} > 0. \tag{27}$$

Equations (26) and (27) prove the enhanced RoCoF and frequency deviation suppression ability of the RPC-based FR strategy with respect to the inertia control. Besides, the suppression ability of maximum frequency deviation can be improved by larger P_{m}.

Besides, by comparing the maxima of: 1) (22) and (15) and 2) (23) and (16), we have

$$\Delta f_{\mathrm{J}}|_{\max} - \Delta f_{\mathrm{D}}|_{\max} = \frac{\Delta P_{\mathrm{L}} K_{\mathrm{D}}}{K_{\mathrm{L}} \left(K_{\mathrm{L}} + K_{\mathrm{D}}\right)} > 0 \tag{28}$$

$$|R_{\mathrm{D}}|_{\max} - |R_{\mathrm{J}}|_{\max} = \frac{\Delta P_{\mathrm{L}} K_{\mathrm{J}}}{T_{\mathrm{J}} \left(T_{\mathrm{J}} + K_{\mathrm{J}}\right)} > 0. \tag{29}$$

Therefore, the droop control always has a better suppression ability of the maximum frequency deviation with respect to the inertia control, whereas the inertia control has a constantly better suppression ability of maximum RoCoF with respect to the droop control.

3) RPC Versus PD Control: Similarly, by substituting (7) into (8), the grid frequency, frequency deviation, and RoCoF under the PD control-based FR strategy can be obtained as

$$f_{\mathrm{PD}} = f_{\mathrm{N}} - \frac{\Delta P_{\mathrm{L}}}{K_{\mathrm{L}} + K_{\mathrm{p}}} \left(1 - e^{-\frac{K_{\mathrm{L}}+K_{\mathrm{p}}}{T_{\mathrm{J}}+K_{\mathrm{d}}} t}\right) \tag{30}$$

$$\Delta f_{\mathrm{PD}} = \frac{\Delta P_{\mathrm{L}}}{K_{\mathrm{L}} + K_{\mathrm{p}}} \left(1 - e^{-\frac{K_{\mathrm{L}}+K_{\mathrm{p}}}{T_{\mathrm{J}}+K_{\mathrm{d}}} t}\right) \tag{31}$$

$$R_{\mathrm{PD}} = -\frac{\Delta P_{\mathrm{L}}}{T_{\mathrm{J}} + K_{\mathrm{d}}} e^{-\frac{K_{\mathrm{L}}+K_{\mathrm{p}}}{T_{\mathrm{J}}+K_{\mathrm{d}}} t}. \tag{32}$$

Substituting (31) and (32) into (7), it is

$$P_{\mathrm{PD}} = \frac{\Delta P_{\mathrm{L}}}{K_{\mathrm{L}} + K_{\mathrm{p}}} \left(K_{\mathrm{p}} + \frac{K_{\mathrm{L}} K_{\mathrm{d}} - T_{\mathrm{J}} K_{\mathrm{p}}}{T_{\mathrm{J}} + K_{\mathrm{d}}} e^{-\frac{K_{\mathrm{L}}+K_{\mathrm{p}}}{T_{\mathrm{J}}+K_{\mathrm{d}}} t}\right) \tag{33}$$

Likewise, to achieve the optimal PD control that provides the maximum FR power yet avoiding saturation, we have

$$\begin{cases} K_{\mathrm{p}} = \dfrac{K_{\mathrm{L}} P_{\mathrm{m}}}{\Delta P_{\mathrm{L}} - P_{\mathrm{m}}} \\ K_{\mathrm{d}} = \dfrac{T_{\mathrm{J}} P_{\mathrm{m}}}{\Delta P_{\mathrm{L}} - P_{\mathrm{m}}} \end{cases} \tag{34}$$

Substituting (34) into (31), (32) and (33) gives rise to

$$\begin{cases} \Delta f_{\mathrm{PD}} \equiv \Delta f_{\mathrm{C}} \\ R_{\mathrm{PD}} \equiv R_{\mathrm{C}} \\ P_{\mathrm{PD}} \equiv P_{\mathrm{C}} \equiv P_{\mathrm{m}} \end{cases} \tag{35}$$

i.e. the FR performance achieved by the RPC strategy is identical to that by the optimal PD control with its parameters given by (34). This is an important conclusion obtained from mathematical proof.

Besides, comparing the maxima of: 1) (11), (15), (22) and (31) and 2) (12), (16), (23) and (32), we have

$$\Delta f_{\mathrm{J}}|_{\max} > \Delta f_{\mathrm{D}}\big|_{\max} = \Delta f_{\mathrm{PD}}|_{\max} = \Delta f_{\mathrm{C}}|_{\max} \tag{36}$$

$$|R_{\mathrm{D}}|_{\max} > |R_{\mathrm{J}}|_{\max} = |R_{\mathrm{PD}}|_{\max} = |R_{\mathrm{C}}|_{\max}. \tag{37}$$

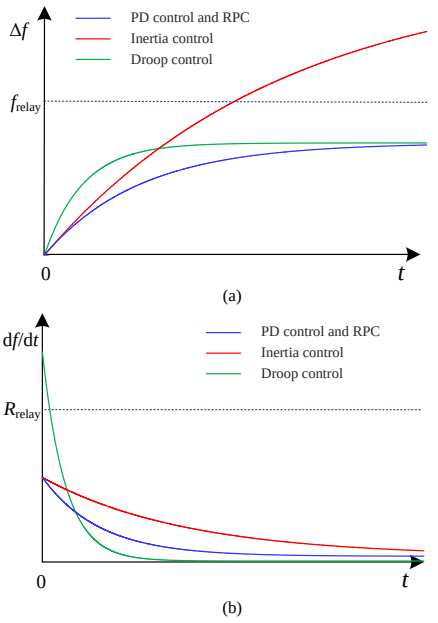

Fig. 3. Performance comparison of four FR strategies with their optimal parameters. (a) Frequency deviation. (b) RoCoF.

It is seen that the RPC scheme and the optimal PD control have prevailing performances in terms of frequency deviation suppression over other schemes, whereas the inertia control has the worst among the four (and thus, the pertinent under/over frequency relays are most likely to be triggered). The RoCoF suppression performances of RPC strategy and the optimal PD control are consistently better than the optimal inertia control, whereas the optimal droop control suffers from the highest probability of RoCoF relays being triggered.

The complete FR performances of the presented RPC strategy and the optimal droop/inertia/PD controls with their pertinent parameters determined by (18), (25) and (34) are illustrated in Fig. 3. Overall, both the RPC scheme and the optimal PD control can significantly reduce the maximum RoCoF value and frequency deviation simultaneously, whereas the other FR strategies can be efficient in merely a single case. Notwithstanding the excellent FR performance provided by the optimal PD control, it requires the controller parameters strictly satisfying (34), which is hardly realized in practice due to the difficulty in determining the grid disturbance ΔP_{L} and T_{J}, K_{L} parameters. On the contrary, the RPC strategy, which has the equivalently optimal FR performance, avoids the use of those unknown grid parameters.

III. Implementation of RPC Based FR Strategy

The driving force of frequency deviation and RoCoF issues, based on the previous analysis, is essentially the grid imbalance power caused by various disturbances. Assuming the case of load power mutation, a sudden load increase or decrease [$\Delta P_{\mathrm{L}} \geq 0$ or $\Delta P_{\mathrm{L}} \leq 0$ in (8)] causes the frequency to drop or increase, and the RoCoF increases with $|\Delta P_{\mathrm{L}}|$. Therefore, the frequency-related indicators can well reflect the power balance of the power system, as illustrated in Fig. 4.

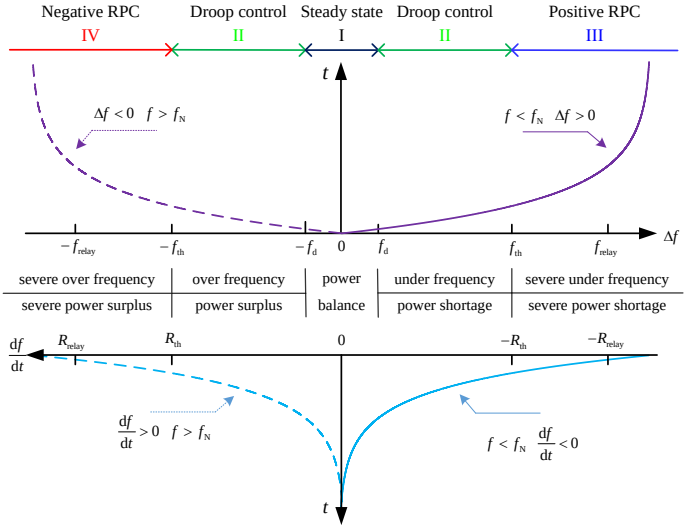

Fig. 4. Relation between frequency indicators and grid power imbalance.

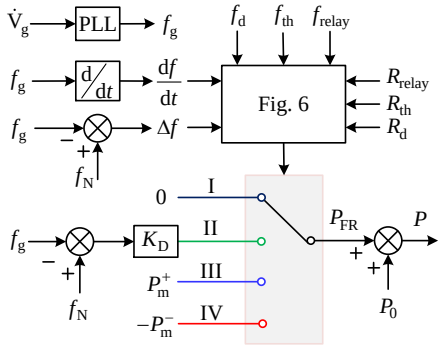

Fig. 5. Inputs, outputs and parameters of the proposed FR scheme.

To alleviate the imbalance power, the FR power provided by generations should satisfy the following.

1) For sudden load power increase and frequency drop [see Fig. 2(a)], generations should provide positive FR power with reference to the direction in Fig. 1 to compensate for the shortage power.
2) Conversely, for sudden load power decrease and frequency rise, generations should provide negative FR power, i.e. they absorb the surplus power.
3) When both RoCoF and frequency deviation approach 0, grid power balance is affirmed, and generations are not required to provide any FR power.

Based on these rules, detailed implementation of the presented strategy can be developed, encompassing four operation modes (see Figs. 5 and 6). Several frequency-related parameters (see Fig. 4) are preliminarily selected to facilitate the mode selection, including the following.

1) f_{d}: Frequency deviation threshold of droop control operation, which is between the measurement noise and the allowed maximum frequency deviation determined by the frequency quality requirement of the grid code.
2) f_{th}: Frequency deviation threshold of RPC operation, which is the allowable maximum value determined by

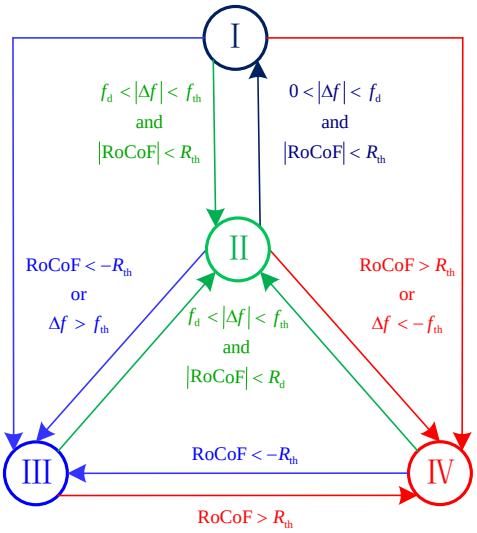

Fig. 6. Working mode transition logic of the proposed FR strategy.

the frequency quality requirement of the grid code.

3) f_{relay}: Threshold of frequency deviation-based relays.
4) R_d: Threshold below which the switching from RPC control mode to droop control mode is allowed.
5) R_{th}: RoCoF threshold of RPC operation.
6) R_{relay}: Threshold of RoCoF based relays.

These parameters satisfy

$$f_{relay} > f_{th} > f_d > 0 \tag{38}$$

$$R_{relay} > R_{th} > R_d > 0 \tag{39}$$

The operation modes of the FR strategy are elaborated as.

1) *Mode I (Steady-State Operation Mode):* For frequency deviation and RoCoF satisfying the grid code requirements, namely, $|df/dt| < R_{th}$ and $|\Delta f| < f_d$, FR service from generations is not required ($P_{FR} = 0$).
2) *Mode II (Droop Control Mode):* For RoCoF meeting the grid code requirement ($|df/dt| < R_{th}$), whereas small frequency fluctuations being present ($f_d < |\Delta f| < f_{th}$), the FR power provided by generations, P_{FR}, is calculated by the droop control in (5) for improved frequency quality. Concerning the constraint imposed by maximum available positive FR power P_m^+ and minimum available negative FR power P_m^- ($P_m^- < 0$), it is

$$P_m^- < P_{FR} < P_m^+. \tag{40}$$

Therefore, the droop coefficient K_D must satisfy

$$K_D < \frac{\min(P_m^+, -P_m^-)}{f_{th}} \tag{41}$$

3) *Mode III (Positive RPC Mode):* For significantly large frequency deviation/RoCoF values close to the grid code protection threshold (namely, $\Delta f > f_{th}$ and/or $df/dt < -R_{th}$), the grid frequency is lower than its rated value f_N and/or continuously falling, and accordingly, generations should provide its maximum available positive FR power ($P_{FR} = P_m = P_m^+ > 0$) to compensate for the severe power shortage, as such reducing the frequency deviation and RoCoF dramatically. Otherwise, if the imbalance power is not suppressed in time, the underfrequency load shedding can be triggered.
4) *Mode IV (Negative RPC Mode):* For $df/dt > R_{th}$ and/or $\Delta f < -f_{th}$, the overfrequency generator disconnection can be triggered if the large frequency deviation and RoCoF are not suppressed rapidly. The grid frequency is greater than f_N and/or continuously rising, suggesting the presence of power surplus to be timely reduced by the minimum negative FR power of generations, namely, $P_{FR} = P_m = P_m^- < 0$. For a generation system without energy storage, $|P_m^-| \le P_0$, whereas in the presence of an energy storage system with rated power P_N, $|P_m^-| \le P_0 + P_N$. It is noted that the FR service in this mode causes electricity output reduction of converters, and hence, price subsidy is required for the auxiliary service market, or the converter participation in the frequency control (P_m^-) should be limited.

It is obvious that Modes III and IV are focused on the efficient reduction of the frequency deviation and RoCoF, by rapidly compensating for the high imbalance power. Mode II aims at improving frequency quality or slowly reducing the FR power to 0 (namely, resuming Mode I) via the droop control when the grid imbalance power is low. The suitable working mode can be selected through the transition logic in Fig. 6.

Note that when analyzing the RPC mode performance and operation conditions, the following prerequisite is defined:

$$0 \le |P_{FR}| \le |P_m| \le |\Delta P_L.| \tag{42}$$

To reliably meet the above condition, R_{th} must satisfy [with H_{min} denoting the minimum system inertia (see Appendix A)]

$$\frac{\max\{P_m^+, -P_m^-\}}{4\pi H_{min}} < R_{th} < R_{relay}. \tag{43}$$

Besides, to achieve the smooth transition from the positive/negative RPC mode to Mode II when the grid imbalance power is low enough, R_d must satisfy (see Appendix B)

$$0 < R_d < R_{th} - \frac{\max\{P_m^+, -P_m^-\}}{4\pi H_{min}} \tag{44}$$

IV. Proposed FR Scheme Verification

In this Section, hardware-in-the-loop (HIL) experiments in a two-converter system with low inertia and simulations in a multimachine grid with normal inertia are utilized to verify the applicability and superiority of the proposed FR scheme. The HIL experimental platform adopted in this work is illustrated in Fig. 7. In the two-converter system (see Fig. 8 and Table II for detailed configuration and parameters), a droop-controlled converter is used to emulate the power grid with voltage and frequency regulation characteristics [27]. For offline simulations, a standard IEEE four-machine two-area (4M2A) system [25] is adopted.

In the experiments, the converter steady-state output power is 0.8 p.u. When providing FR service, the converter forward and reverse adjustment capacities are 0.2 p.u. and 0.1 p.u., respectively, which are the limits of FR power for any FR strategy. Besides, the PD controller is adopted as the reference

TABLE II
PARAMETERS OF THE LOW-INERTIA TWO-CONVERTER POWER SYSTEM

Parameter	Value	Parameter	Value
Rated line-to-line voltage E_0	380 Vrms	Z_g	0.12 Ω / 0.2 mH
Rated grid frequency	50 Hz	Passive filter	0.01 Ω / 0.1 mH
Rated grid active power P_{ref}	20 kW	DC voltage U_{DC}	800 V
Rated grid reactive power Q_{ref}	0 kVar	Current loop: K_p	0.24
Load power	36 kW	Current loop: K_i	2.5
Active power loop: K_P	7.6E-5	Voltage loop: K_p	0.2
Reactive power loop: K_Q	3.1E-3	Voltage loop: K_i	280

TABLE III
FR CONTROLLER PARAMETERS ADOPTED IN EXPERIMENT

Scenario	Single Disturbance	Multiple Disturbances
Droop control	$K_p = 25$, $K_d = 1$	$K_p = 21$, $K_d = 2$
Inertia control	$K_p = 2$, $K_d = 7$	$K_p = 5$, $K_d = 8$
PD control	$K_p = 25$, $K_d = 7$	$K_p = 21$, $K_d = 8$

implementation for FR strategies other than the proposed one. The droop and inertia schemes are emulated by adjusting the derivative and proportional gains of the PD control.

A. Single Disturbance Scenario in Two-Converter System

As the load power suddenly increases by 0.36 p.u., the grid frequency continuously drops in the absence of converter FR strategy and finally reaches a new steady state [see Fig. 9(a)]. This natural FR serves as the baseline for comparison of the aforementioned FR schemes. Among them, controller parameters for optimal inertia/droop/PD strategies that achieve maximum FR power output are obtained via repeated trial (see Table III). The parameters adopted in the proposed strategy are listed in Table IV.

TABLE IV
FREQUENCY RELATED PARAMETERS ADOPTED IN EXPERIMENT

Parameter	Value	Parameter	Value	Parameter	Value
f_d	0.05 Hz	f_{th}	0.22 Hz	f_{relay}	0.6 Hz
R_d	0.5 Hz/s	R_{th}	1.5 Hz/s	R_{relay}	2.5 Hz/s

As a preliminary observation, experimental results in Fig. 9 proved the significance of FR service. In the absence of FR service from the generation, the frequency drops drastically in the event of load power mutation, with frequency nadir of 49.38 Hz [see Fig. 9(a)] and maximum absolute RoCoF of 4.375 Hz/s [see Fig. 9(c)]. Such a critical case easily triggers

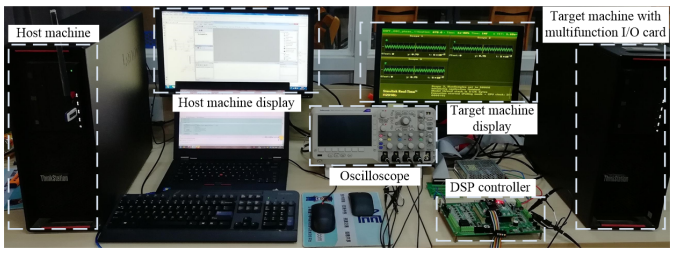

Fig. 7. Hardware-In-the-Loop experimental platform.

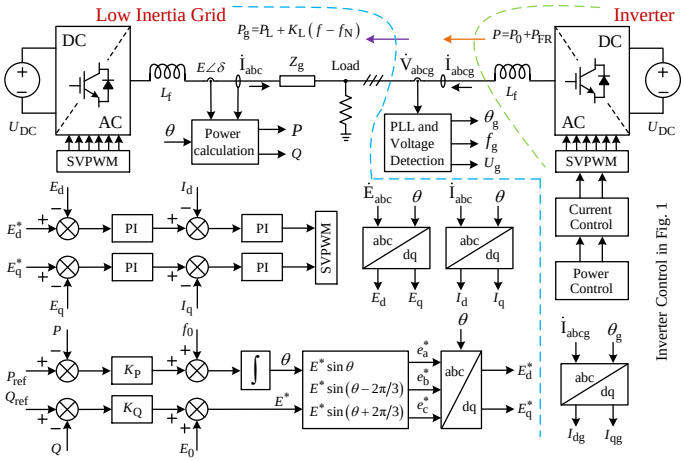

Fig. 8. Configuration of the two-converter system for FR performance test.

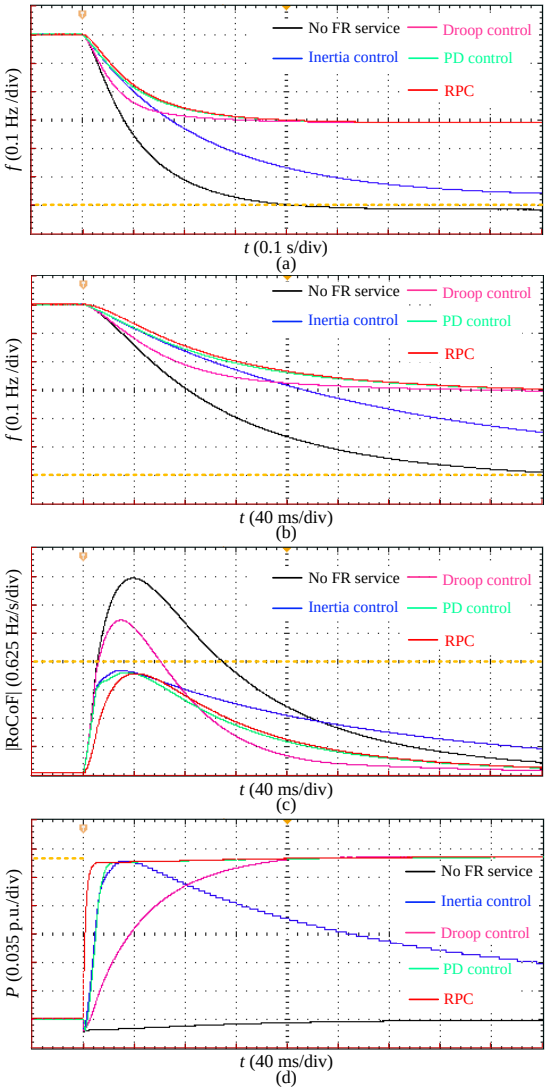

Fig. 9. Experiment results in single disturbance scenario. (a) and (b) Frequency dynamics in 0.9 s and 0.36 s. (c) RoCoF. (d) Converter output FR power.

frequency related relays, yet it can be effectively avoided

by adopting FR strategies for the converter. Specifically, the maximum RoCoF with the droop control (3.44 Hz/s) is slightly larger with respect to the inertia control (2.31 Hz/s), yet the frequency nadir with droop control (49.7 Hz) is notably higher versus that with inertia control (49.44 Hz). When a steady state is reached, the frequency deviation with droop control (about 0.3 Hz) is much smaller with respect to the inertia control (about 0.56 Hz). Indeed, since the inertia control is inactive ($P_{\mathrm{FR}} \approx 0$) in steady state, its pertinent frequency deviation is almost consistent with that of the natural FR. In contrast, the PD control and the proposed RPC-based strategy are able to adequately diminish the frequency deviation and RoCoF simultaneously while improving the frequency nadir, providing optimal performances for all the indicators of interest (the pertinent frequency deviation, maximum RoCoF, and frequency nadir are 0.3 Hz, 2.3 Hz/s, and 49.7 Hz, respectively).

The result of converter output FR power in Fig. 9(d) is as well consistent with the analyses in Sections II and III. Upon the load power increase, the RoCoF is initially large, whereas the frequency deviation is small, and hence, the inertia control can provide much significant FR power with respect to droop control. In the frequency nadir zone, the RoCoF decreases with nonnegligible frequency deviation caused by frequency drifting from the nominal value, and the resulting FR power output with the inertia control is smaller with respect to the droop control. When the RPC-based strategy or the optimal PD control is adopted, the full capacity of generation FR power can be utilized to compensate for the imbalance power, as such greatly alleviating the frequency deviation and RoCoF issues and enhancing the frequency quality. Experiment results in Fig. 9 also demonstrated the identical FR performance achieved by the RPC strategy and the optimal PD control, yet the latter has to be realized by repeated parameter tuning.

B. Multiple Disturbance Scenario in 2-Converter System

To verify the superiority of the RPC-based FR service under different working conditions, three consecutive disturbances, i.e., a slight one with 0.1-p.u. load power increase, and two large ones with 0.3-p.u. load power increase and 0.4-p.u. load power drop, are introduced in the experiment, causing two grid frequency declines and one frequency rise.

Fig. 10 demonstrates the FR result of the power grid under the effect of inertia/droop/PD control and RPC scheme. It is obvious that slight power disturbance causes insignificant system RoCoF and frequency deviation, and the converter FR power is relatively small under all FR strategies. However, during the subsequent disturbances with bulky power drop and increase, the frequency will rapidly drop or increase if the generation provides insufficient FR service. Especially, a large power drop causes the frequency nadir down to 49.3 Hz [see Fig. 10(a)], which significantly exceeds the triggering threshold of the underfrequency relay; two consecutive large disturbances in opposite directions result in RoCoF maximum values up to 3.6 Hz/s and 5.0 Hz/s [see Fig. 10(b)], respectively, significantly exceeding the triggering threshold of over-RoCoF relays. The severe frequency deviation and RoCoF issues caused by the two large disturbances extremely increase the probability of frequency related relays being triggered and sharply weaken the system's ability to maintain continuous and stable operation. The role played by the FR strategy is of paramount importance under such conditions.

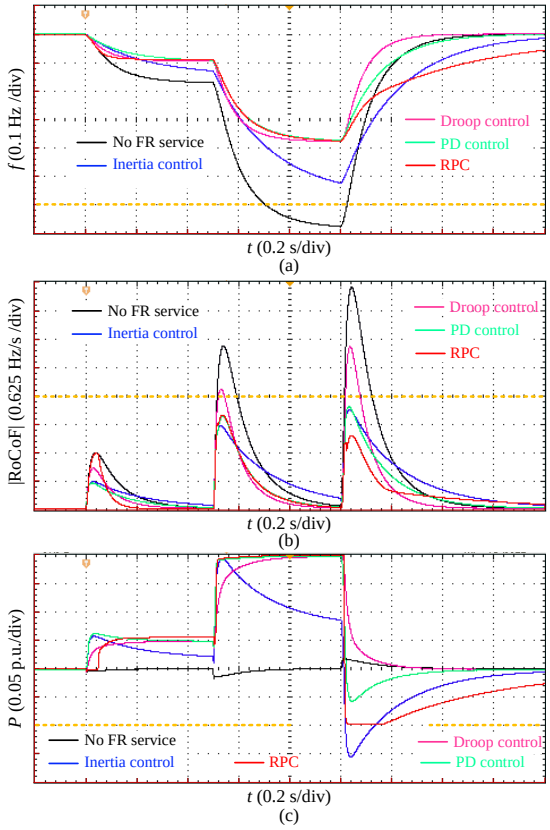

Fig. 10. Experiment results in the multiple disturbance scenario. (a) Frequency dynamic process. (b) RoCoF. (c) Converter output FR power.

To improve the system FR features quickly and effectively, the imbalance power caused by various disturbances should be compensated as soon as possible. The classic controls and the proposed RPC scheme enable the converter to actively provide FR power in response to the frequency change caused by power imbalance (see Fig. 10). For consistency, the parameters of inertia/droop/PD control (see Table III) are determined under the same condition of excessive power drop, ensuring that the converter forward regulation power does not exceed 0.2 p.u. when providing FR service.

When the converter adopts the inertia control, the system inertia is significantly strengthened. With bulky power increase, the RoCoF is reduced from 3.6 to 1.88 Hz/s [see Fig. 10(b)], which is below the action threshold of over-RoCoF relays. However, the controller effect on frequency deviation is not obvious, and the frequency nadir still approaches the triggering threshold of the underfrequency relay [see Fig. 10(a)]. In view of imbalance power reduction, the FR power output from the generation, which is proportional to the RoCoF in this case, becomes insignificant as the RoCoF decreases, thus making it less effective for limiting the frequency nadir. Under the condition of a drastic power drop, though the RoCoF is reduced from 5.0 to 2.25 Hz/s [see Fig.10(b)] and the over-RoCoF relay triggering is avoided, the FR power

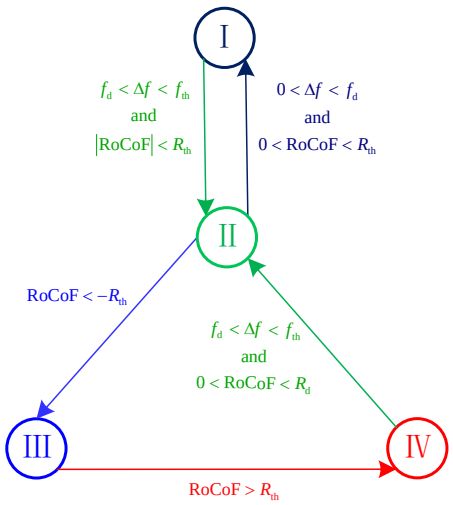

Fig. 11. Working mode transition logic of the experimental scenario.

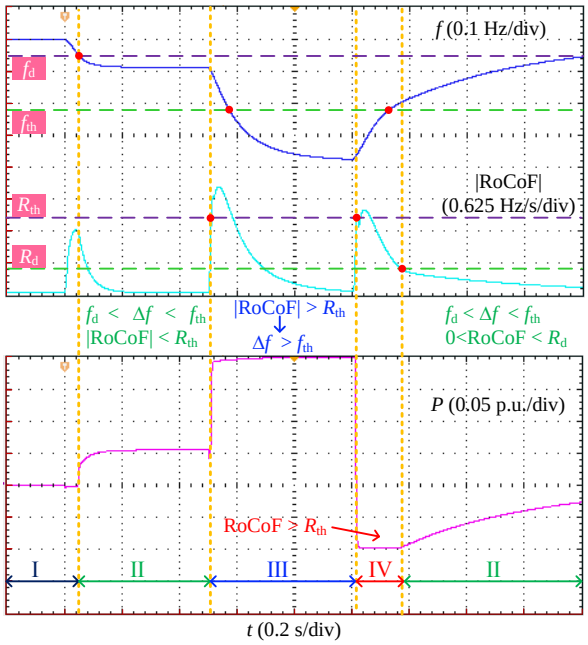

Fig. 12. Experiment results with the proposed RPC control.

exceeds the reverse adjustment range (0.1 p.u.) [see Fig.10(d)]. Hence, inertia control parameters that maximize the RoCoF suppression under a certain condition cannot guarantee the best performance is also achieved under other working conditions, while satisfying the allowable power range of the converter.

Conversely, when the droop control is used, the suppression ability of system frequency deviation can be enhanced significantly. The provided FR power is always proportional to the frequency deviation [see Fig. 10(c)], effectively improving the frequency nadir and, thereby, reducing the risk of triggering over/underfrequency relays. However, the RoCoF suppression ability is weaker with respect to the previous case. Indeed, the maximum RoCoF values caused by two large disturbances are as high as 2.6 and 3.6 Hz/s, respectively [see Fig. 10(b)], which significantly exceeds the triggering threshold of RoCoF relays.

When the PD control is adopted, significantly improved FR features of the power grid can be observed in the event of drastic power increase, ascribed to the optimal parameter tuning under this condition. As a matter of fact, both the frequency deviation and RoCoF have been effectively suppressed, namely, the frequency nadir (49.52 Hz) is above the underfrequency relay threshold, and the RoCoF (2.1 Hz/s) is lower than the RoCoF relay threshold, thereby effectively avoiding these relays being triggered. Meanwhile, its FR performance is equivalent to the proposed RPC-based FR strategy in this case. However, under the condition of a drastic power drop, the FR performance with PD control is not optimized, and the result is significantly worse than that with the proposed method. Analogously, fine-tuned PD control parameters merely guarantee the optimal FR performance in a specific operating condition.

Finally, when the RPC based FR strategy is adopted, the FR features of the power grid have been significantly improved, and the FR performance is the best in all operating conditions. In this scenario, the converter-based generation successively explores modes pertinent to steady-state operation (Mode I), droop control (Mode II), positive RPC (Mode III), negative RPC (Mode IV), droop control (Mode II), and steady-state operation (Mode I), as shown in Fig. 11. Regardless of the disturbance applied, the RPC-based strategy always accurately determines whether the system is in power shortage or surplus based on real-time information of frequency, frequency deviation, and RoCoF, meanwhile outputting maximized FR power to compensate for the imbalance power or improving the frequency quality (see Fig. 12). Accordingly, the frequency deviation and RoCoF can be suppressed quickly and efficiently [see Fig. 10(a) and (b)], significantly lowering the risk of frequency-related relays being triggered.

C. Verification in Complex Multi-Machine System

Effectiveness of the proposed scheme under different disturbances are verified in the IEEE 4M2A system with nonlinear and reactive loads (see Fig. 13), by comprehensive comparison versus the two most representative FR schemes, i.e. the PD control with extensive industrial applications and the swing-equation-based VSG control popular in academic researches. The simulations are also divided into small- and large-disturbance scenarios. The load is suddenly increased by 25 MW at 40 s for small-disturbance condition and increased by 90 MW at 52 s for the large-disturbance condition.

Analogously, the converter power limit is considered for all involved FR strategies. Specifically, by setting the converter capacity limit to 150 MW and the steady-state transmission power to 100 MW, the maximum available capacity for FR service is merely 50 MW. The control parameters for PD- and VSG-based strategies are designed accordingly. The results of system frequency, RoCoF and inverter output power measured at bus B2 are compared in Fig. 14, validating the applicability and superiority of the RPC-based FR service in the complex multimachine power system. It is noted that the IEEE 4M2A system is dominated by SGs characterized by large inertia, and

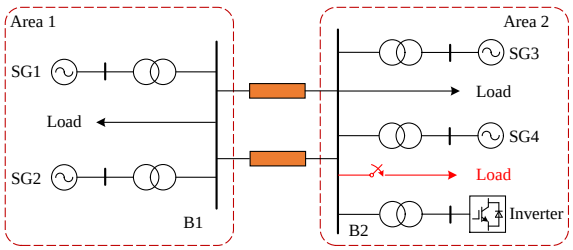

Fig. 13. Configuration of the IEEE 4M2A system for the FR performance test.

hence, the RoCoF issue is less severe than in the low-inertia two-converter system in Fig. 8.

In addition, it is worth mentioning that the complex power oscillation [see Fig. 14(c)] associated with the swing-equation-based VSG schemes is a major issue that restricts their practical application, and hence, many adaptive versions have been proposed to alleviate this issue to a certain extent. Indeed, such an issue is unavoidable when accounting for the extremely limited converter capacity for FR service, leading to a poor FR performance (even worse than that without an FR service) and the risk of system desynchronization. The pertinent system instability mechanism can be found, e.g., in [26]–[28].

Conversely, an enhanced VSG scheme with sufficiently large inertia and damping parameters contributes to effective reduction in oscillations [from 80 to about 13 MW in Fig. 15(c)] and incomparable FR performance [see Fig. 15(a) and (b)], yet it leads to excessive FR power [80 MW in Fig. 15(c), which is beyond the maximum available capacity of 50 MW] and the over-current fault. Hence, it is difficult to obtain a good compromise for the abovementioned contradiction through parameter design of the swing-equation-based VSG schemes.

In summary, both the simulation and experiment verification have proved the superiority of the RPC-based FR strategy in terms of: 1) effectively avoiding the complex oscillations associated with swing-equation-based VSG strategies; 2) significantly reducing the maximum RoCoF value and frequency deviation simultaneously compared with classic PD-based FR schemes; and 3) ensuring the provided FR power does not exceed the allowable range under all operating conditions.

V. Conclusion

This article proposes the RPC-based FR strategy with detailed implementation, and its enhanced performance in suppressing the frequency deviation and RoCoF during the frequency transient is proved by comparison versus classic control methods, under the identical allowable capacity constraint. The main conclusions are as follows:

1) The inertia of the power system is weakened by bulk injection of constant power converters, causing frequency deviation and RoCoF relays to be triggered easily and further consequences to occur. Accordingly, grid-tied converters need to take the responsibility to maintain system stability, by providing suitable FR service, especially in low-inertia power systems.

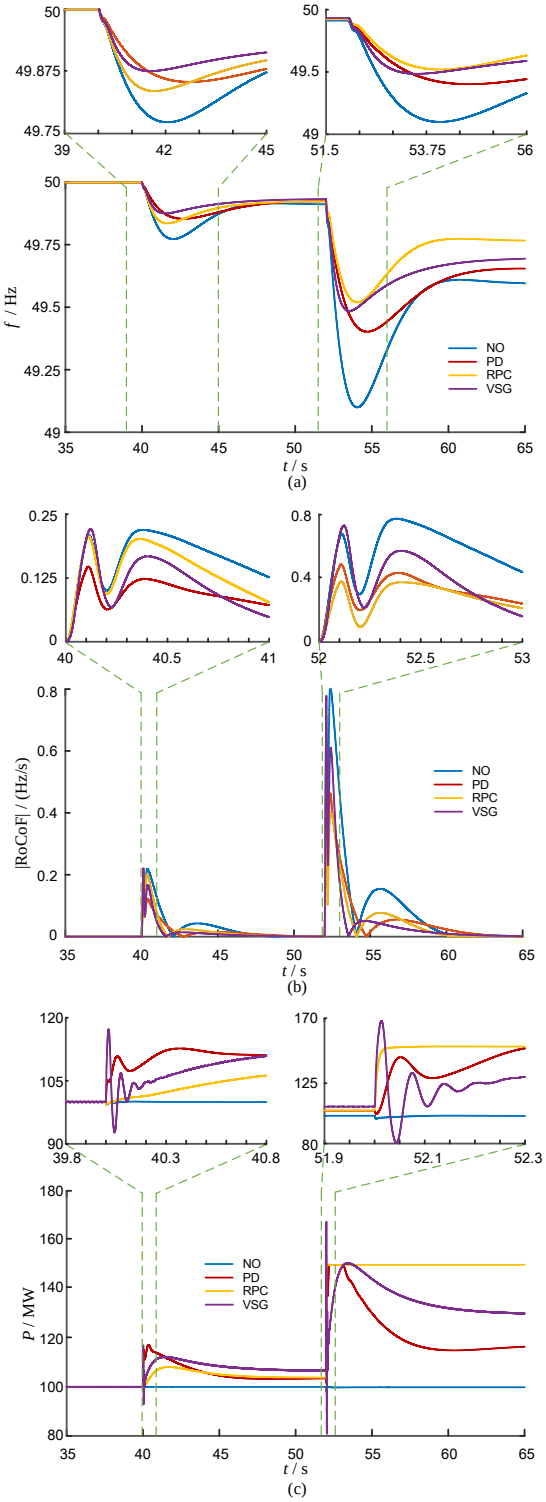

Fig. 14. (a) Frequency, (b) absolute RoCoF, and (c) active power dynamics of the studied 4M2A system with different FR schemes.

2) The proposed FR strategy can effectively avoid the complex oscillations associated with swing-equation-based VSG schemes and provide the optimal frequency deviation/RoCoF suppression ability with respect to the classic inertia/droop/PD control, by decoupling the FR power from frequency deviation/RoCoF and directly

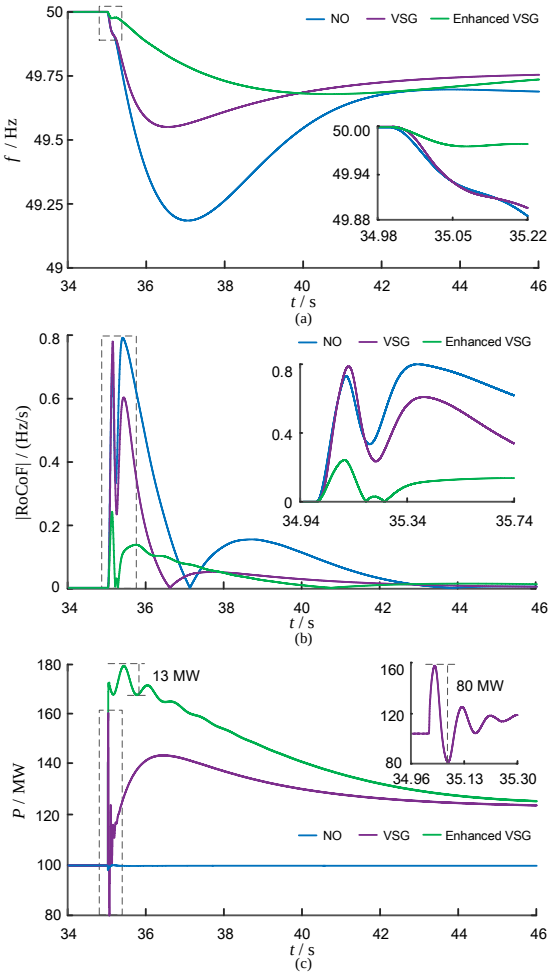

Fig. 15. (a) Frequency, (b) absolute RoCoF and (c) active power dynamics of the studied 4M2A system with two VSG implementations.

compensating for the imbalance power to its maximum extent. Comparison results verified its effectiveness.

3) Based on real-time information of frequency, frequency deviation and RoCoF, the proposed RPC-based FR strategy rapidly and accurately determines the grid imbalance power direction and adjusts the converter working mode, and its feasibility is proved via experiment results.
4) The classic inertia/droop/PD controls with given parameters cannot achieve the theoretically optimal FR performance under various operating conditions. Conversely, the optimal FR performance can be easily achieved by the proposed method with the pertinent parameters readily determined by the grid code.

Although not considered here for the sake of simplicity, it is also worth mentioning that stability assessment of the proposed model can be accomplished with additional efforts of inverter output impedance analysis for different operation modes and accounting for various influential factors inside the system, e.g. the inverter topology and structural parameters, passive filter and its parameters, the phase-locked loop, and the current/frequency control loops and their parameters. As a matter of fact, the proposed control has good stability and applicability in most grid environments, provided that a reasonable grid structural design is satisfied.

APPENDIX A
PROOF OF R_{TH} CONSTRAINT

First, the critical disturbance power P_{critical} is defined, yielding

$$|P_{\text{critical}}| = \lambda |P_{\text{m}}| \tag{45}$$

where $\lambda > 1$ is a certain safety factor.

According to (1), the system RoCoF at this critical disturbance power P_{critical} ($P_{\text{im}} = |P_{\text{critical}}|$) is

$$R_{\text{th}} = \frac{|P_{\text{critical}}|}{4\pi H} = \frac{\lambda |P_{\text{m}}|}{4\pi H} > \frac{|P_{\text{m}}|}{4\pi H}. \tag{46}$$

When the system imbalance power P_{im} occurs due to a sudden disturbance power $|\Delta P_{\text{L}}|$, i.e., $P_{\text{im}} = |\Delta P_{\text{L}}|$, the system frequency will change according to (1), and its RoCoF is

$$R = \left|\frac{\mathrm{d}f}{\mathrm{d}t}\right| = \frac{|\Delta P_{\text{L}}|}{4\pi H}. \tag{47}$$

When the detected grid RoCoF, R, is greater than R_{th}, namely

$$R > R_{\text{th}}, \tag{48}$$

substitution of (46) and (47) into (48) gives

$$\frac{|\Delta P_{\text{L}}|}{4\pi H} > \frac{\lambda |P_{\text{m}}|}{4\pi H} \Rightarrow |\Delta P_{\text{L}}| > \lambda |P_{\text{m}}| > |P_{\text{m}}|. \tag{49}$$

In such a case, the disturbance power $|\Delta P_{\text{L}}|$ must be greater than the maximum adjustment capacity of the converter $|P_{\text{m}}|$, i.e. the condition in (42) is satisfied, and the system can immediately switch to the RPC control mode.

The maximum FR power provided by the converter corresponds to the forward or reverse adjustment range, i.e. P_{m} takes the values of P_{m}^{+} or P_{m}^{-}. Besides, the grid inertia H is proportional to the system capacity, which can be predicted by the daily/annual load curve. Accordingly, the grid inertia coefficient fluctuates within a certain range, i.e.

$$H_{\min} < H < H_{\max}. \tag{50}$$

Considering (46) to be valid within the variable ranges of the P_{m} and H parameters, it holds that

$$R_{\text{th}} > \max\left(\frac{|P_{\text{m}}|}{4\pi H}\right) = \frac{\max\{P_{\text{m}}^{+}, -P_{\text{m}}^{-}\}}{4\pi H_{\min}} \tag{51}$$

By combing (39) and (51), (43) can be obtained.

APPENDIX B
PROOF OF R_{D} CONSTRAINT

According to the proof in Appendix A, when the system satisfies $|R| > R_{\text{th}}$ condition [see (48)], the disturbance power $|\Delta P_{\text{L}}|$ must be greater than the critical disturbance power P_{critical} ($|\Delta P_{\text{L}}| > |P_{\text{critical}}|$), suggesting the presence of severe imbalance power P_{im} in the system, which will cause obvious RoCoF and frequency deviation issues and high probability of triggering protection relays. Even if the converter RPC strategy is executed immediately and the system imbalance power is

reduced from $|\Delta P_{\mathrm{L}}|$ to $(|\Delta P_{\mathrm{L}}| - |P_{\mathrm{m}}|)$, the imbalance power is still present, yielding

$$|\Delta P_{\mathrm{L}}| - |P_{\mathrm{m}}| > |P_{\mathrm{critical}}| - |P_{\mathrm{m}}| = (\lambda - 1)\,|P_{\mathrm{m}}| > 0. \quad (52)$$

After the converter fully exploits its FR power and supports the system operation, the inherent grid regulation capability will continue to stabilize frequency and further reduce the imbalance power until power balance is reached at a new frequency operation point. During this process, the system imbalance power will gradually decrease from $(|\Delta P_{\mathrm{L}}| - |P_{\mathrm{m}}|)$ to a smaller value, $|P_{\mathrm{im\_c}}|$ (and $|P_{\mathrm{im\_c}}| < |\Delta P_{\mathrm{L}}| - |P_{\mathrm{m}}|$). At this time, the corresponding RoCoF index, R, yields

$$R = \frac{|P_{\mathrm{im\_c}}|}{4\pi H} \quad (53)$$

When $|P_{\mathrm{im\_c}}|$ is small enough, the converter can exit the RPC mode when appropriate (e.g. by switching to the steady-state or droop operation mode). Considering the worst case, i.e. the converter directly switches from the RPC mode to steady-state operation mode that does not provide any FR power, the system imbalance power will suddenly increase from $|P_{\mathrm{im\_c}}|$ to $(|P_{\mathrm{im\_c}}| + |P_{\mathrm{m}}|)$. At this time, to avoid jitters and ensure the converter does not return to the RPC mode, it must be ensured that the system imbalance power after converter switching to the new mode $(|P_{\mathrm{im\_c}}| + |P_{\mathrm{m}}|)$ to be less than the critical power required to start the RPC mode, i.e.,

$$|P_{\mathrm{im\_c}}| + |P_{\mathrm{m}}| < |P_{\mathrm{critical}}|\,. \quad (54)$$

By dividing both sides of (54) by $4\pi H$ and considering (46) and (53), it is

$$R < R_{\mathrm{d}} = R_{\mathrm{th}} - \frac{|P_{\mathrm{m}}|}{4\pi H}. \quad (55)$$

Accordingly, when the detected RoCoF meets the requirement in (55), the converter can be switched to the new mode and be guaranteed not to return to the original RPC mode.

Though (55) is designed according to the worst condition, in this article, the FR power provided by the converter is controlled and must not directly drop from P_{m} to 0 (i.e. a direct transition from Mode III or IV to Mode I is prohibited) but, instead, gradually reduced through droop control (Mode II), in line with the grid frequency regulation requirements. Hence, a sufficient margin is present in (55) to avoid the controller bouncing between Mode III/IV and Mode II.

In addition, for (55) to be constantly valid within the parameter perturbation range, we have

$$R_{\mathrm{d}} < \min\left(R_{\mathrm{th}} - \frac{|P_{\mathrm{m}}|}{4\pi H}\right) = R_{\mathrm{th}} - \frac{\max\{P_{\mathrm{m}}^{+}, -P_{\mathrm{m}}^{-}\}}{4\pi H_{\mathrm{min}}} \quad (56)$$

By combing (39) and (56), (44) can be obtained.

REFERENCES

[1] European Network of Transmission System Operators for Electricity (ENTSO-E) and Operators for electricity, "Continental Europe Significant Frequency Deviations - January 2019," ENTSO-E aisbl, Brussels, Belgium, Tech. Rep.

[2] "IEEE Guide for the Application of Protective Relays Used for Abnormal Frequency Load Shedding and Restoration," IEEE Standard C37.117-2007, Aug. 2007, pp. 1-55.

[3] Australian Energy Market Operator (AEMO), "Black system South Australia 28 September 2016," AEMO, Melbourne, VIC, Australia, Tech. Rep., Mar. 2017, available: https://www.aemo.com.au/energy-systems/electricity/national-electricity-market-nem/nem-events-and-reports/power-system-operating-incident-reports.

[4] J. C. Vieira, W. Freitas, W. Xu, and A. Morelato, "Efficient coordination of ROCOF and frequency relays for distributed generation protection by using the application region," *IEEE Trans. Power Del.*, vol. 21, no. 4, pp. 1878–1884, 2006.

[5] P. Energy, "Rate of change of frequency (ROCOF)-review of TSO and generator submissions final report," Commission for Energy Regulation (CRU) Report N.20353, May 2013.

[6] Brian Mulhern, "Rate of Change of Frequency (RoCoF) Modification to the Grid Code," Utility Regulator, Tech. Rep., 2014, available: https://www.uregni.gov.uk/news-centre/rate-change-frequency-rocof-modification-grid-code.

[7] S. Wei, Y. Zhou, G. Xu, and Y. Huang, "Motor-generator pair: A novel solution to provide inertia and damping for power system with high penetration of renewable energy," *IET Gener. Transm. Distrib.*, vol. 11, no. 7, pp. 1839–1847, 2017.

[8] M. Liserre, R. Teodorescu, and F. Blaabjerg, "Stability of photovoltaic and wind turbine grid-connected inverters for a large set of grid impedance values," *IEEE Trans. Power Electron.*, vol. 21, no. 1, pp. 263–272, 2006.

[9] E. Du, N. Zhang, B.-M. Hodge *et al.*, "The role of concentrating solar power toward high renewable energy penetrated power systems," *IEEE Trans. Power Syst.*, vol. 33, no. 6, pp. 6630–6641, 2018.

[10] R. Domínguez, A. J. Conejo, and M. Carrión, "Toward fully renewable electric energy systems," *IEEE Trans. Power Syst.*, vol. 30, no. 1, pp. 316–326, 2014.

[11] S. Wei, Y. Zhou, and Y. Huang, "Synchronous motor-generator pair to enhance small signal and transient stability of power system with high penetration of renewable energy," *IEEE Access*, vol. 5, pp. 11 505–11 512, 2017.

[12] H.-P. Beck and R. Hesse, "Virtual synchronous machine," in *Proc. 9th Int. Conf. Elect. Power Qual. Utilisation*, 2007, pp. 1–6.

[13] Q.-C. Zhong and G. Weiss, "Synchronverters: Inverters that mimic synchronous generators," *IEEE Trans. Ind. Electron.*, vol. 58, no. 4, pp. 1259–1267, 2011.

[14] W. Zhang, D. Remon, and P. Rodriguez, "Frequency support characteristics of grid-interactive power converters based on the synchronous power controller," *IET Renew. Power Gener.*, vol. 11, no. 4, pp. 470–479, 2017.

[15] X. Meng, J. Liu, and Z. Liu, "A generalized droop control for grid-supporting inverter based on comparison between traditional droop control and virtual synchronous generator control," *IEEE Trans. Power Electron.*, vol. 34, no. 6, pp. 5416–5438, 2019.

[16] F. Wang, L. Zhang, X. Feng, and H. Guo, "An adaptive control strategy for virtual synchronous generator," *IEEE Trans. Ind. Appl.*, vol. 54, no. 5, pp. 5124–5133, 2018.

[17] M. A. Torres L., L. A. C. Lopes, L. A. Morán T., and J. R. Espinoza C., "Self-tuning virtual synchronous machine: A control strategy for energy storage systems to support dynamic frequency control," *IEEE Trans. Energy Convers.*, vol. 29, no. 4, pp. 833–840, 2014.

[18] A. Karimi, Y. Khayat, M. Naderi *et al.*, "Inertia response improvement in AC microgrids: A fuzzy-based virtual synchronous generator control," *IEEE Trans. Power Electron.*, vol. 35, no. 4, pp. 4321–4331, 2020.

[19] D. Li, Q. Zhu, S. Lin, and X. Bian, "A self-adaptive inertia and damping combination control of VSG to support frequency stability," *IEEE Trans. Energy Convers.*, vol. 32, no. 1, pp. 397–398, 2017.

[20] J. Alipoor, Y. Miura, and T. Ise, "Power system stabilization using virtual synchronous generator with alternating moment of inertia," *IEEE J. Emerg. Sel. Top. Power Electron.*, vol. 3, no. 2, pp. 451–458, 2015.

[21] J. Alipoor, Y. Miura, and T. Ise, "Stability assessment and optimization methods for microgrid with multiple VSG units," *IEEE Trans. Smart Grid*, vol. 9, no. 2, pp. 1462–1471, 2018.

[22] S. D'Arco and J. A. Suul, "Equivalence of virtual synchronous machines and frequency-droops for converter-based microgrids," *IEEE Trans. Smart Grid*, vol. 5, no. 1, pp. 394–395, 2014.

[23] M. Farrokhabadi, C. A. Cañizares, J. W. Simpson-Porco *et al.*, "Microgrid stability definitions, analysis, and examples," *IEEE Trans. Power Syst.*, vol. 35, no. 1, pp. 13–29, 2020.

[24] H. T. Nguyen, G. Yang, A. H. Nielsen, and P. H. Jensen, "Combination of synchronous condenser and synthetic inertia for frequency stability enhancement in low-inertia systems," *IEEE Trans. Sustain. Energy*, vol. 10, no. 3, pp. 997–1005, 2019.

[25] J. M. Mauricio, A. Marano, A. Gómez-Expósito, and J. L. M. Ramos, "Frequency regulation contribution through variable-speed wind energy conversion systems," *IEEE Trans. Power Syst.*, vol. 24, no. 1, pp. 173–180, 2009.

[26] L. Xiong, F. Zhuo, F. Wang *et al.*, "Static synchronous generator model: A new perspective to investigate dynamic characteristics and stability issues of grid-tied PWM inverter," *IEEE Trans. Power Electron.*, vol. 31, no. 9, pp. 6264–6280, Sep. 2016.

[27] L. Huang, H. Xin, Z. Wang *et al.*, "Transient stability analysis and control design of droop-controlled voltage source converters considering current limitation," *IEEE Trans. Smart Grid*, vol. 10, no. 1, pp. 578–591, 2019.

[28] H. Wu and X. Wang, "A mode-adaptive power-angle control method for transient stability enhancement of virtual synchronous generators," *IEEE J. Emerg. Sel. Top. Power Electron.*, vol. 8, no. 2, pp. 1034–1049, 2020.

[29] D. Yang, X. Wang, F. Liu *et al.*, "Adaptive reactive power control of PV power plants for improved power transfer capability under ultra-weak grid conditions," *IEEE Trans. Smart Grid*, vol. 10, no. 2, pp. 1269–1279, 2020.

[30] N. Hatziargyriou, J. Milanović, C. Rahmann *et al.*, "Stability definitions and characterization of dynamic behavior in systems with high penetration of power electronic interfaced technologies," IEEE Power and Energy Society, Piscataway, NJ, USA, Tech. Rep., Apr. 2020, PES-TR77.